Catal Lett (2008) 126:293–300
DOI 10.1007/s10562-008-9613-3

Selective Oxidation and Oxidative Dehydrogenation of Isobutane over Hydrothermally Synthesized Mo–V–O Mixed Oxide Catalysts

Jingqi Guan · Haiyan Xu · Ke Song · Bo Liu · Fanpeng Shang · Xiaofang Yu · Qiubin Kan

Received: 12 July 2008 / Accepted: 7 August 2008 / Published online: 3 September 2008

Abstract A series of Mo–V–O catalysts were prepared by calcining the orthorhombic (M1) Mo–V–O phase containing precursors under different conditions ($T = 500$ or 600 °C in atmosphere of N_2 or air) and tested for the oxidation of isobutane and isobutene. Characterization results (BET, XRD, XPS, FTIR, and TPR) showed that their structure and properties depend on the composition of the calcined samples and the calcined conditions. Catalytic tests showed that relatively high isobutane conversion and desired product selectivity can be achieved over $MoV_{0.3}$-500-N and $MoV_{0.3}$-600-A catalysts. It is also found that both orthorhombic M1 phase and $(V_{0.07}Mo_{0.93})_5O_{14}$ phase are active and selective for the selective oxidation of isobutane to methacrolein, whereas higher selectivity toward methacrolein (40.4%) can be achieved over the former phase at a moderate isobutane conversion (6.4%). Moreover, $(Mo_{0.3}V_{0.7})_2O_5$ phase may be propitious to complete oxidation for the selective oxidation of isobutane. On the other hand, the presence of V affects the activity and selectivity, and a low surface V^{4+} concentration prefers selective oxidation products. In addition, specific surface areas of the catalysts appear to be little important in determining the catalytic activation.

Keywords Isobutane · Isobutene · Selective oxidation · Methacrolein · Mo–V–O mixed oxide catalysts

J. Guan · H. Xu · K. Song · B. Liu · F. Shang · X. Yu · Q. Kan
College of Chemistry, Jilin University, Changchun 130023, People's Republic of China

Q. Kan (✉)
Jiefang Road 2519, Changchun 130021, People's Republic of China
e-mail: catalysischina@yahoo.com.cn; qkan@mail.jlu.edu.cn

1 Introduction

Isobutane is one of the most important components in natural gas and crude oil, but it has not been widely used up to now. In the past decades, studies have focused mainly on one-step oxidation of isobutane to partial oxidation products via Keggin-type heteropolyoxometallate compounds [1–5] or mixed oxide catalysts [6–10]. Methacrolein (MAL) and methacrylic acid (MAA) are the key intermediates in one of the existing processes for the production of methyl methacrylate. Although the conventional catalytic process from isobutene to MAA and multistep catalytic oxidation reaction of acetone with hydrogen cyanide show a very high yield of MAA [11–13], developing catalysts for the direct oxidation of isobutane to MAL and MAA is needed for optimal use of this abundant resource.

Mo-based and V-based oxides have been most widely used for catalytic activity of light alkanes (C_1–C_5) [10, 14–19]. It is well known that molybdenum oxide-based and vanadium oxide-based systems are generally reducible metal oxides, in which a heterogeneous redox-type mechanism prevails for the partial oxidation of hydrocarbons. In these catalytic systems, the control of the redox properties of Mo and V is the key point for the development of active and selective species. The redox properties of Mo or V can be modified by introducing some metal or nonmetal elements to form multicomponent systems. In addition, the formation of molecular-type compounds is another route to control the redox properties of Mo or V, in which the properties of the basic structural unit can be adjusted through the composition of the compound itself. For example, the redox properties of Mo can be considerably improved by the formation of the Keggin structure with the elements of phosphorus and oxygen [20].

Mo–V–based systems have been proven effective for selective oxidation of C_2–C_4 alkanes, especially for ethane and propane [15–17]. For instance, one of the best Mo–V–Te–Nb–O oxide catalysts is able to convert propane directly into the acrylic acid with a selectivity of 68% at a propane conversion of 37% at 400 °C [16]. These materials are characterized by the presence of an active and selective crystalline phase, that is, the orthorhombic TeM_3O_{10} (M = Mo, V and Nb), the so-called M1 phase [21]. Additionally, other crystalline phases, such as pseudohexagonal M2 ($Te_2M_{20}O_{57}$) phase, might act as assistant phases to enhance the selectivity of acrylic acid [22]. However, the exact stoichiometry and structure of all possible active and selective component(s) in the mixture of phases of Mo–V-based system and variants of structures it contains is still the object of a debate. It is therefore necessary that further investigators should be carried out due to many questions are still to be solved.

Very recently, Mo–V-based catalysts have been reported to be potential catalysts for the selective oxidation of isobutane to MAL and MAA [8–10]. For example, 7.8% of yield to MAL can be achieved over a $MoV_{0.3}Te_{0.23}Sb_{0.5}O_x$ catalyst [8], while 10.7% of total yield to MAL and MAA can be obtained over a $MoV_{0.3}Te_{0.23}Ce_{0.2}O_x$ catalyst [10]. However, there is no orthorhombic M1 phase in the catalysts by the dry-up method, and the catalytic performance over these catalysts is still poor because a feasibility report of this process shows that a minimum of 35% yield in MAL and MAA is required for its commercialization (Brazdil JF, Private communication, 1997). It is thereby strongly hoped that catalysts containing high active and selective phases for the selective oxidation of isobutane should be designed.

It has now been found that several novel mixed metal oxide catalysts, which may be prepared by a hydrothermal synthesis technique, may be utilized for the partial oxidation of an alkane, or a mixture of an alkane and an alkene, to produce an unsaturated carboxylic acid; or for the ammoxidation of an alkane, or a mixture of an alkane and an alkene, to produce an unsaturated nitrile [23–33]. For instance, an examination of several methods for preparing Mo–V–Te–Nb–O mixed oxides found that hydrothermal treatment was shown to give a precursor of a propane ammoxidation catalyst which shows activity twice as high, after calcination, as the catalyst prepared by the known dry-up method [34]. These observations confirmed the fact that the redox properties of Mo and V can be considerably adjusted through the composition of the compound itself by a hydrothermal synthesis route to produce molecular-type compounds like M1 and M2 phases, which in return improved the catalytic performance of the Mo–V–Te–Nb–O system.

In this paper, we used a hydrothermal method to prepare Mo–V–O mixed metal oxides with different V/Mo atom ratio, which were calcined under different conditions (T = 500 or 600 °C in atmosphere of N_2 or air). Both bulk and surface cases were investigated. Results showed that crystalline phases might be modified depending on the nominated amount of each element and the calcined conditions. Moreover, with similar phase compositions, obvious changes in the performance of catalysts demonstrating that the role of vanadium is as a significant redox element and an important relationship exists between the V^{5+}/V^{4+} pair and catalytic performance.

2 Experimental

2.1 Catalyst Preparation

Hydrothermal conditions were used for preparing the crystalline Mo–V–O complex metal oxides [34]. In a typical synthesis, in 30 mL of water heated at 80 °C, 3.60 g of MoO_3, 0.68 g of V_2O_5, and 7.5 mmol of oxalic acid, were added to form a slurry. The slurry was introduced into a stainless autoclave equipped with a Teflon® inner tube and then the autoclave was heated at 175 °C for 48 h. After cooling, the solid obtained was separated by filtration and washed with water several times, and dried at 110 °C for 12 h to give a black solid. The sample will be denoted as $MoV_{0.3}$, which was calcined under a flow of N_2 (50 mL/min) or air (50 mL/min) to obtain the catalyst. The calcination was performed with a heating rate of 2 °C/min. The final calcination temperature was 500 °C for 2 h or 600 °C for 2 h. The samples will be designed as $MoV_{0.3}$-X-Y, where X indicates the final calcination temperature (500 or 600 °C) and Y indicates the gas used during the calcination step (A = Air and N = N_2).

For comparative purpose, MoO_3 was prepared in the same manner as the MoV catalysts.

2.2 Catalyst Characterization

The specific surface areas of the catalysts were measured based on the adsorption isotherms of N_2 at −196 °C using the BET method (Micromeritics ASAP2010). Powder X-ray diffraction (XRD) patterns were collected using a Shimadzu XRD-6000 scanning at 4°/min with Cu$K\alpha$ radiation (40 kV, 30 mA). The infrared spectra (IR) of various samples were recorded at room temperature using a NICOLET Impact 410 spectrometer.

X-ray photoelectron spectra (XPS) were recorded on a VG ESCA LAB MK-II X-ray electron spectrometer using Al$K\alpha$ radiation (1,486.6 eV, 10.1 kV). The spectra were referenced with respect to the C 1s line at 284.7 eV. The measurement error of the spectra was ±0.2 eV.

H_2-temperature programmed reduction (TPR) experiments were carried out in a flow reactor system, in which 10 mg of catalyst was charged each run into a U-shaped quartz microreactor (4 mm i.d.). After purging with Ar gas from 50 to 300 °C at a ramp rate of 10 °C/min, holding at 300 °C for 30 min, and cooling to 100 °C, the sample was reduced in a 5% H_2/Ar stream (25 mL/min). The reduction temperature was raised uniformly from 100 to 800 °C at a ramp of 10 °C/min. H_2 consumption was measured by a thermal conductivity detector (TCD).

2.3 Catalytic Tests

The reaction was performed in a stainless steel tubular fixed bed reactor (16 mm i.d., 400 mm long) under atmospheric pressure. Each catalytic test was carried out using 1.0 g of catalyst, which was granulated into particles of 20–30 mesh size and diluted with 1.0 g of SiC particles to prevent temperature gradients and hot spots in the reactor. Under our reaction conditions, the homogeneous reaction can be neglected. Carbon mass balances of ≥97% were typically observed.

The feed was controlled by a mass flow controller, and water was fed by a mini-pump. The catalytic reaction condition was as follows: molar ratio of the feed gas i-C_4H_{10}:O_2:N_2:H_2O = 2:1:1.6:1.4, i-C_4H_8:O_2:N_2:H_2O = 1:2:5:2. The products were then fed via heated lines to an on-line gas chromatography for analysis. Isobutene (i-$C_4^=$), methacrolein (MAL), CO_x (CO, CO_2), acetic acid (HAC) propylene ($C_3^=$), acetone, methacrylic acid (MAA), acrolein, and acrylic acid were detected as products.

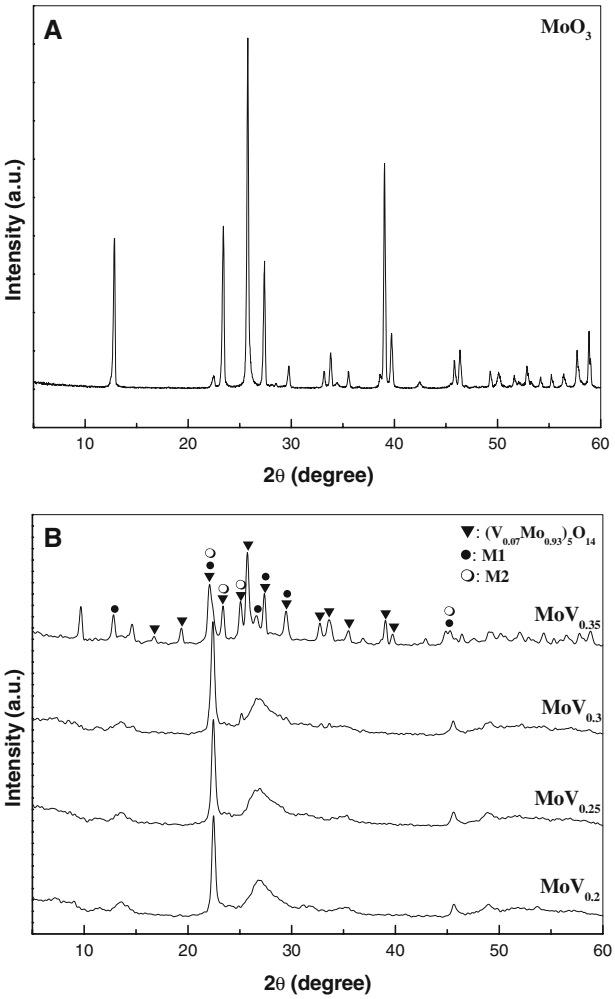

Fig. 1 XRD patterns of as-synthesized samples

3 Results and Discussion

3.1 XRD Studies

Figure 1 shows the patterns of the as-synthesized samples. As can be seen from Fig. 1a, the MoO_3 prepared by the hydrothermal route did not change its crystal structure [JCPDS 35-0609]. In other words, the orthorhombic M1 phase was not formed without the addition of vanadium into the MoO_3 system. The formation of the orthorhombic (M1) Mo–V–O phase was investigated over a range of synthesis V/Mo ratios from 0.2 to 0.35 (Fig. 1b). The catalysts prepared at the synthesis V/Mo ratios of 0.2, 0.25 and 0.3 showed the presence of mainly orthorhombic M1 phase with lattice parameter (a = 21.10 Å, b = 26.57 Å, c = 4.006 Å) [35, 36]. However, the synthesis molar V/Mo ratio of 0.35 was found to produce many structural variants including M1 phase, $(V_{0.07}M_{0.93})_5O_{14}$ [JCPDS 31-1437] and pseudohexagonal M2 phase [37–39]. In addition, the intensities of the peaks corresponding to orthorhombic M1 phase (especially of the peak at 26.6°) decreased with increasing synthesis V/Mo ratio suggesting that the relative content of M1 phase decreased, while the intensities of the peaks attributed to pseudohexagonal M2 phase (especially of the peak at 25.3°) increased with increasing synthesis V/Mo ratio displaying the relative increase of this phase.

Figure 2 provides the XRD patterns of Mo–V–O mixed oxide catalysts calcined under different conditions. For the samples calcined in air, the peaks at 2θ = 13.0°, 23.6°, 26.0°, 27.6°, 33.4°, 34.0°, 35.7°, and 39.2° can be assigned to MoO_3 [JCPDS 35-0609], whereas the peaks at 2θ = 13.0°, 18.6°, 21.8°, 26.0°, and 33.4° can be attributed to Mo_4O_{11} [JCPDS 13-0142]. Moreover, the peaks at 2θ = 15.0°, 25.3°, 26.0°, 29.8°, and 33.1° can be ascribed to $(Mo_{0.3}V_{0.7})_2O_5$ [JCPDS 21-0576], and the peaks at 2θ = 21.8°, 22.2°, 25.3°, 26.0°, 27.6°, 33.1°, 33.4°, and 39.2° can be related to $(V_{0.07}M_{0.93})_5O_{14}$ [JCPDS 31-1437]. In contrast, the XRD pattern of the samples calcined in N_2 indicates the presence of MoO_3, Mo_4O_{11}, $(Mo_{0.3}V_{0.7})_2O_5$,

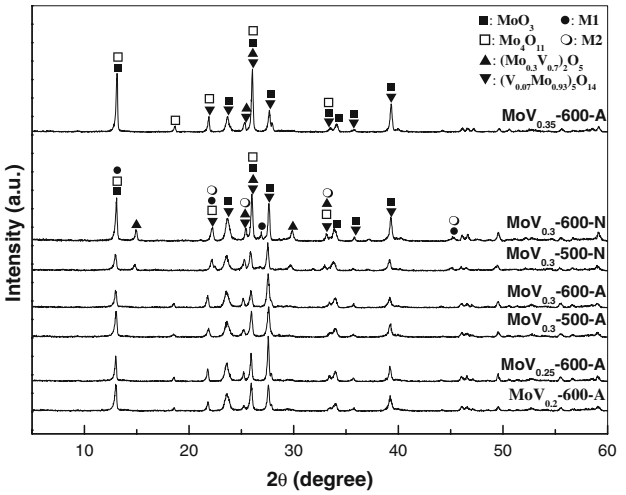

Fig. 2 XRD patterns of Mo–V–O mixed oxide catalysts calcined under different conditions

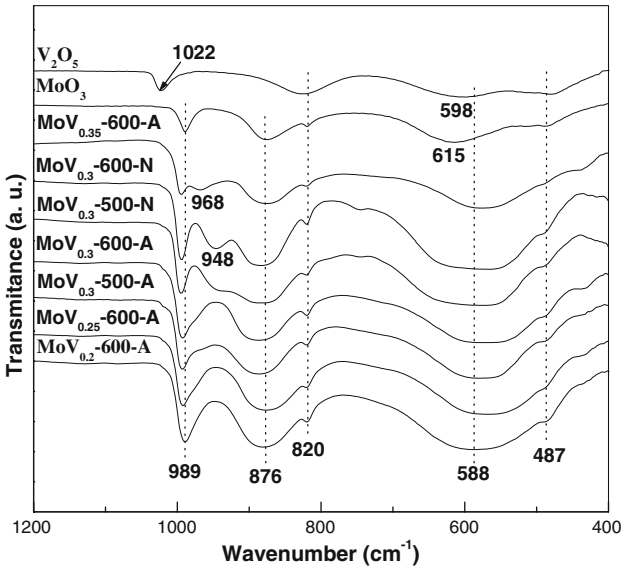

Fig. 3 IR spectra of MoO_3, V_2O_5 and Mo–V–O mixed oxide catalysts calcined under different conditions

$(V_{0.07}M_{0.93})_5O_{14}$, and two new crystalline phases: orthorhombic M1 phase ($2\theta = 13.0°$, 22.2°, 26.9°, and 45.2°), and pseudohexagonal M2 phase ($2\theta = 22.2°$, 25.3°, 33.1°, and 45.2°) [37]. Considering that there are both M1 and M2 phases in all of the as-synthesized samples, it can be concluded that the structures of M1 and M2 phases have been destroyed by calcination in air, while these phases can be partially reserved after calcination in N_2, which is in agreement with other reports [36, 37].

In addition, it can be found that the relative content of Mo_4O_{11} ($2\theta = 18.6°$) decreased, whereas the relative content of V-rich phase of $(Mo_{0.3}V_{0.7})_2O_5$ ($2\theta = 15.0°$) increased when the samples were calcined under N_2 compared with the catalysts calcined under air stream. Furthermore, one can find from the XRD patterns of the samples calcined under air at 600 °C that the content of Mo–V-containing phases relatively increases, while the content of MoO_n phases relatively decreased with increasing V/Mo ratio from 0.2 to 0.3.

3.2 FTIR Studies

Figure 3 displays the IR spectra of MoO_3, V_2O_5 and Mo–V–O mixed oxide catalysts calcined under different conditions. It is obvious that the bands at 989, 876, 820, 615, and 487 cm^{-1} are characteristic of MoO_3. However, all of these bands can be shifted from their original positions due to incorporation of V atoms to the system [40]. In the meanwhile, the bands at 1,022, 823, 598, and 487 cm^{-1} are characteristic of V_2O_5.

For the samples calcined in air, the bands at 989, 876, 820, and 487 cm^{-1} can be attributed to MoO_3, whereas the band at 968 and 588 cm^{-1} should be related to Mo–O–V bond [10]. In addition, the FTIR spectra of samples calcined in N_2 are similar to those calcined in air, except that a new band at 948 cm^{-1} appears which can be ascribed to a new Mo–O–V bond (e.g. the Mo–O–V bond in M1 or M2 phase according to XRD results).

3.3 XPS Studies

To gain deeper insight into the surface constitution and properties of these catalysts, their Mo $3d_{5/2}$ and V $2p_{3/2}$ binding energies were investigated and corresponding spectra were composed and integrated with the results shown in Table 1. The Mo $3d_{5/2}$ peak of catalysts could be fitted into two components at 231.7 and 232.8 eV, which can be assigned to Mo^{5+} and Mo^{6+} species, respectively [10]. Thus, small amount of Mo^{5+} ions were found on the surface of the $MoV_{0.3}$ catalyst calcined in N_2, while almost no Mo^{5+} ion was observed on the surface of the Mo–V–O catalysts calcined in air, suggesting that the coordinatively unsaturated Mo^{5+} was pronely oxidized to Mo^{6+} under oxidizing atmosphere. Combined with the XRD results, it can be concluded that there is no M1 or M2 crystallite in the catalysts calcined in air because the average oxidation state of the M cations is approximately the same in the two phases, +5.33 in M1 and +5.3 in M2, which means that a part of the molybdenum cations have a +5 oxidation state [22].

The V $2p_{3/2}$ peak of catalysts could be fitted into two components at 516.2 and 517.3 eV, which can be related to V^{4+} and V^{5+} species, respectively [40]. A greater amount of V^{4+} was present on the $MoV_{0.3}$-500-A and $MoV_{0.3}$-600-N catalysts surface than on the $MoV_{0.3}$-500-N and $MoV_{0.3}$-600-A catalysts surface.

Table 1 Binding energies and surface atomic ratios calculated from XPS data on the catalysts calcined under different conditions

Sample	Binding energy (eV)			Surface composition (at.%)				Surface oxidation states	
	Mo $3d_{5/2}$	V $2p_{3/2}$	O 1s	Mo	V	O	V/Mo	Mo^{5+}/Mo^{6+}	V^{4+}/V^{5+}
$MoV_{0.2}$-600-A	233.1	517.6	531.7	18.4	3.3	78.3	0.18	0/1	0.06/0.94
$MoV_{0.25}$-600-A	233.1	517.5	531	18.3	3.4	78.3	0.19	0/1	0.07/0.93
$MoV_{0.3}$-500-N	232.9	516.9	530.8	20.2	3.9	75.9	0.19	0.05/0.95	0.01/0.99
$MoV_{0.3}$-600-N	232.9	516.9	530.8	26.7	3.9	69.4	0.15	0.06/0.94	0.18/0.82
$MoV_{0.3}$-500-A	233.0	517.4	530.8	21.4	5.4	73.2	0.25	0/1	0.28/0.72
$MoV_{0.3}$-600-A	233.1	517.5	530.9	20.5	4.2	75.3	0.20	0/1	0.03/0.97
$MoV_{0.35}$-600-A	233.1	517.5	530.8	17.7	4.6	77.7	0.26	0/1	0.10/0.90

3.4 H_2-TPR Studies

H_2-TPR profiles of MoO_3, V_2O_5 and Mo–V–O mixed oxide catalysts calcined under different conditions are shown in Fig. 4. The TPR profile of pure V_2O_5 displayed two peaks at 659 and 705 °C, corresponding to the step-wise reduction of $V_2O_5 \rightarrow 1/3V_6O_{13}$ and $1/3V_6O_{13} \rightarrow 2VO_2$, respectively [41]. Moreover, there were two peaks of H_2-consumption with two maxima at 674 and 742 °C for pure MoO_3, corresponding to the stepwise reduction of $MoO_3 \rightarrow MoO_2$ and $MoO_2 \rightarrow$ Mo, respectively [10, 42, 43]. As it can be seen, the H_2-TPR profiles of all the samples calcined under air displayed a main peak at around 700 °C, considered to be associated with the reduction of $MoO_3 \rightarrow MoO_2$ and $V_6O_{13} \rightarrow 6VO_2$. However, synergetic effects between the Mo and V ions in the reduction procedure can not be neglected. Additionally, for the sample $MoV_{0.3}$ calcined under N_2 stream at 500 and 600 °C, the main TPR peaks appeared at about 675 °C, lower than those samples calcined under air, which were mainly considered to be due to the reduction of Mo^{6+}-species [10].

3.5 Catalytic Properties

The effect of reaction temperature was investigated at GHSV = 2,800 mL h^{-1} g_{cat}^{-1} and i-C_4H_{10}:O_2 = 2:1 (mol). The catalytic results obtained by changing reaction temperature in the range 350–440 °C are plotted in Fig. 5. As expected, conversion increased with temperature. However, conversion was very low (<3.0%) below 370 °C and grew rapidly up to about 10.0% at 370 °C, afterward it slightly increased. These results demonstrate that the optimal activation temperature for isobutane over $MoV_{0.3}$-600-A catalyst should be above 370 °C. In the meanwhile, the selectivity toward isobutene reached a maximum at 370 °C, which gradually decreased with the increase of reaction temperature. On the other hand, the selectivity to MAL simultaneously increased with the increase of temperature from 370 to 420 °C, and then it decreased with further increasing reaction temperature due to its overoxidation. The results above support the hypothesis that the oxidative dehydrogenation of isobutane to isobutene is the first step in the selective oxidation of isobutane to MAL

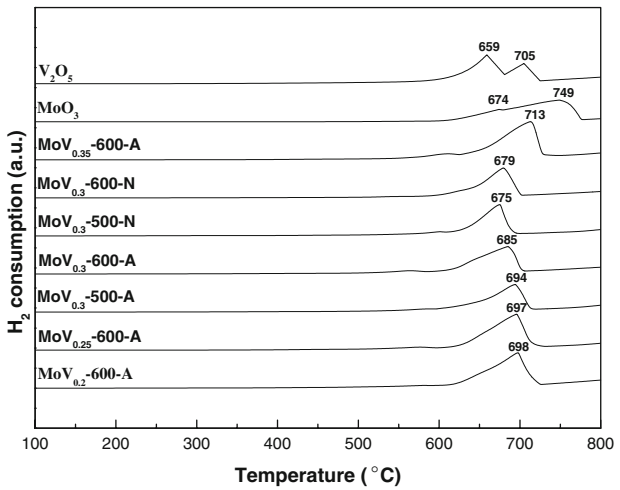

Fig. 4 H_2-TPR profiles of MoO_3, V_2O_5 and Mo–V–O mixed oxide catalysts calcined under different conditions

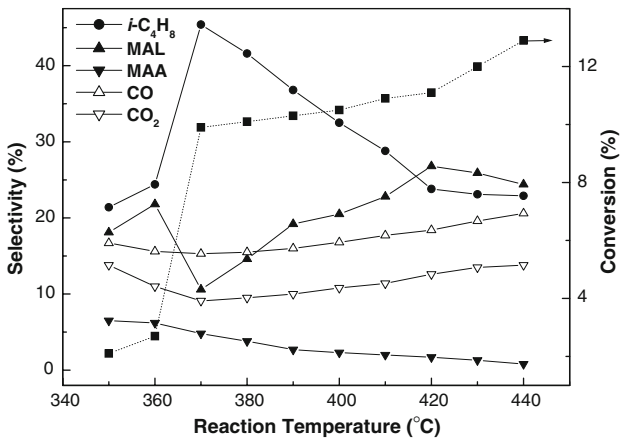

Fig. 5 Conversion/selectivity versus the reaction temperature obtained during the oxidation of isobutane over $MoV_{0.3}$-600-A. Experimental conditions: i-C_4H_8:O_2:N_2: H_2O = 2:1:1.6:1.4 (mol); GHSV = 2,800 h^{-1}

and then the isobutene intermediate is oxidized to MAL, which is in good agreement with our previous report [8].

In addition, the CO and CO_2 selectivities increased with increasing reaction temperature from 370 to 440 °C, whereas the selectivity to MAA decreased with raising reaction temperature, indicating that MAA is pronely oxidized to CO_x at relatively high temperature over Mo–V–O catalysts.

The catalytic results obtained for the oxidation of isobutane over the catalysts at 420 °C, given in Table 2, indicate that the MoO_3 catalyst was active and selective for the partial oxidation of isobutane to MAL. Moreover, for the samples calcined in air at 600 °C, the selectivity to MAL and MAA was improved considerably by the addition of small amounts of vanadium to the Mo-based system. For example, the selectivity to MAL and MAA reached 22.5 and 1.5%, respectively, at V/Mo ratios as low as 0.2. The MAL and MAA selectivities increased continuously with increasing vanadium content, reaching a maximum (26.8% MAL selectivity and 1.7% MAA selectivity) at a V/Mo ratio of 0.3. However, the MAL and MAA selectivities decreased with further increases in vanadium content. It should be noted that the catalytic performance over the catalysts prepared by the hydrothermal synthesis method is generally better than those synthesized by a sol–gel synthesis route, in which only 0.6% selectivity to MAL can be achieved at a very low isobutane conversion (2.6%) over a $Mo_{50}V_{50}O_x$ catalyst [44].

In addition, obviously the highest selectivity to isobutene and the lowest selectivity to MAL and MAA could be obtained over V-free catalyst MoO_3. Thus, it can be concluded that the incorporation of vanadium into the Mo-based system had a positive effect on the transformation of isobutene to MAL and MAA in the selective oxidation of isobutane [10].

In the meantime, the effects of calcined conditions on the possible active phases and catalytic behavior of $MoV_{0.3}$ catalyst were also evaluated, and the results are reported in Table 2. The conversion of isobutane over the $MoV_{0.3}$-500-N is the lowest, while the maximum conversion can be obtained over the $MoV_{0.3}$-600-A catalyst. The selectivity to isobutene and MAL could be considerably affected by the calcined temperature and atmosphere. For instance, the maximum selectivity to isobutene can be achieved over $MoV_{0.3}$-600-A catalyst, whereas the maximum selectivity to MAL has been attained over $MoV_{0.3}$-500-N. Besides, relatively high selectivity toward MAA should be obtained over the catalysts calcined under N_2 stream. Thereby, it seems that molybdenum may be the key element for the activation of isobutane, whereas the selective oxidation of isobutene to MAL might proceed mainly on the surface of the Mo–V-containing crystalline phase (e.g. $(V_{0.07}M_{0.93})_5O_{14}$). A close examination of the XRD patterns of $MoV_{0.3}$-500-N and $MoV_{0.3}$-600-A catalysts showed that there is orthorhombic M1 phase in the $MoV_{0.3}$-500-N catalyst, while this phase is absent in the $MoV_{0.3}$-600-A catalyst. According to some previous references [15–17], the orthorhombic M1 phase was found to be active and selective for propane (amm)oxidation. Our experimental results lead to a similar conclusion that isobutene oxidation to MAL might occur over the M1 phase. Moreover, it has been reported that in the selective oxidation of propane over Mo–V–Sb–Nb–O catalyst, the presence of $(M_xMo_{1-x})_5O_{14}$ (M = V or Nb) favors the formation of acrylic and acetic acid [45, 46]. This proposal is also supported by our experimental results, however, as shown in Table 2, we found that the phase appears to be very low selective for the selective oxidation of isobutane to MAA.

In contrast, the catalytic results shown in Table 2 show that the selectivities to isobutene and MAL over $MoV_{0.3}$-500-A and $MoV_{0.3}$-600-N catalysts were very low. Combined with XRD results, it can be inferred that higher V-containing phase $(Mo_{0.3}V_{0.7})_2O_5$ was present in $MoV_{0.3}$-600-N catalyst than in $MoV_{0.3}$-500-N catalyst, while the catalytic performance for the former was far worse than the latter. Therefore, it can be suggested that the presence of $(Mo_{0.3}V_{0.7})_2O_5$ phase in the catalysts should not be propitious to the formation of MAL, but favor the complete oxidation. Furthermore, it can be found that there is higher $(V_{0.07}M_{0.93})_5O_{14}/MoO_n$ ratio in $MoV_{0.3}$-600-A catalyst

Table 2 Catalytic properties of the catalysts for isobutane oxidation at 420 °C[a]

Catalysts	S_{BET} ($m^2\ g^{-1}$)	Conversion (%)	Selectivity (%)							
			i-$C_4^=$	MAL	MAA	CO	CO_2	$C_3^=$	ACT	HAC
MoO_3	0.8	7.4	58.2	10.6	0	10.2	5.2	7.7	4.4	3.5
$MoV_{0.2}$-600-A	0.1	9.7	28.2	22.5	1.5	18.9	12.9	6.1	2.2	7.5
$MoV_{0.25}$-600-A	0.4	10.4	26.4	24.1	1.6	18.6	12.7	6.3	2.1	8.0
$MoV_{0.3}$-500-N	10.5	6.4	5.4	40.4	3.1	20.5	14.6	6.5	0.8	8.5
$MoV_{0.3}$-600-N	4.2	9.0	6.6	13.7	3.4	28.4	24.9	3.8	1.1	17.9
$MoV_{0.3}$-500-A	5.8	9.6	2.8	10.8	1.0	33.2	30.6	4.3	0.5	16.6
$MoV_{0.3}$-600-A	3.8	11.1	23.8	26.8	1.7	18.4	12.6	6.9	2.0	7.6
$MoV_{0.35}$-600-A	0.5	8.5	20.5	24.6	1.6	22.5	13.2	6.1	1.2	10.1

[a] Operating condition: GHSV = 2,800 mL h^{-1} g_{cat}^{-1}, P = 101 kPa

than in $MoV_{0.3}$-500-A catalyst. As discussed above, $(V_{0.07}M_{0.93})_5O_{14}$ phase might be helpful to convert the isobutene intermediate to produce MAL, which leads to the expectation that higher MAL selectivity was obtained over $MoV_{0.3}$-600-A catalyst than over $MoV_{0.3}$-500-A catalyst.

In addition, MAL selectivity was strongly affected by the V^{4+}/V^{5+} surface atomic ratio in the calcined catalysts. As it can be seen from Table 1, far higher surface V^{4+}/V^{5+} ratios are detected in $MoV_{0.3}$-500-A (0.28/0.72) and $MoV_{0.3}$-600-N (0.18/0.82) than those in $MoV_{0.3}$-500-N (0.01/0.99) and $MoV_{0.3}$-600-A (0.03/0.97) catalysts. Nevertheless it is clear that the catalytic behavior over the catalysts with high surface V^{4+}/V^{5+} ratios was worse than the ones with low surface V^{4+}/V^{5+} ratios. It indicated that high surface V^{5+}/V^{4+} ratio in the Mo–V–O catalysts favored the formation of MAL and vanadium acted as a redox element in surface: $V^{5+} + Mo^{5+} \leftrightarrow V^{4+} + Mo^{6+}$. Zhu et al. also reported similar results, demonstrating that the selectivity of acrolein over a $MoV_{0.3}Te_{0.25}O_x$ catalyst decreased when surface and bulk V^{4+} increased [47].

BET specific surface areas of the catalysts prepared for this study were also listed in Table 2. One can find that the effect of specific surface area was not the determining factor for the selective oxidation of isobutane to MAA over Mo–V–O catalysts.

The reaction results of selective oxidation from isobutene to MAL over the catalysts at 420 °C are summarized in Table 3. It can be seen that MoO_3 presents a low isobutene conversion and MAL selectivity. The conversion of isobutene increased with the addition of V into Mo-based system. One should pay attention to the fact that the specific surface area of the samples varies with the V content and that the isobutene conversion changes may not be mainly due to the changes in specific surface area. For example, 41.1% of isobutene conversion could be achieved over $MoV_{0.2}$-600-A catalyst with as low as 0.1 $m^2\ g^{-1}$ of specific surface area, whereas only 38.4% of isobutene conversion could be achieved over $MoV_{0.35}$-600-A catalyst with as high as 0.5 $m^2\ g^{-1}$ of specific surface area. For the sample $MoV_{0.3}$, it was very similar to the catalytic results of isobutane oxidation that the selectivity to MAL was lower over $MoV_{0.3}$-500-A and $MoV_{0.3}$-600-N catalysts than over $MoV_{0.3}$-600-A and $MoV_{0.3}$-500-N catalysts. This finding again proved the suggestion that Mo–V-containing phases like $(V_{0.07}M_{0.93})_5O_{14}$ and the orthorhombic M1 phase might be active and selective for partial oxidation of isobutene, while the V-rich phase $(Mo_{0.3}V_{0.7})_2O_5$ was favorable for complete oxidation.

In addition, it can be concluded that the selectivity to MAL in the selective oxidation of isobutene over Mo–V–O catalysts is generally higher than that in the selective oxidation of isobutane. Therefore, it is reasonable to propose that MAL is formed from isobutene. However, the reaction pathway for the oxidation of isobutane directly from isobutane or an intermediate cannot be excluded. In other words, MAL is formed following a parallel-consecutive scheme: the consecutive path of the reaction may include the steps: isobutene → MAL → MAA → CO_x. The extent of the successive reactions will increase with the increase in total conversion of isobutane.

4 Conclusion

Activated Mo–V–O catalysts were obtained by calcining hydrothermally synthesized MoV_x ($x = 0.2$–0.35) precursors. The composition of the calcined samples and the calcination conditions strongly influence the nature of crystalline phases, reducibility, surface composition, and the catalytic performance of these materials in the title reaction. The Mo–V-containing phases ($(V_{0.07}M_{0.93})_5O_{14}$ and orthorhombic M1 phase) are suggested to be active and selective for isobutane oxidation, while V-rich phase $(Mo_{0.3}V_{0.7})_2O_5$ is related to the formation of CO_x. In addition, the orthorhombic M1 phase is found to be more selective to MAL for selective oxidation of isobutane than $(V_{0.07}M_{0.93})_5O_{14}$. Furthermore, higher selectivity to MAL can be attained over the catalysts with high surface V^{5+}/V^{4+} ratio, while the catalysts having more surface V^{4+} is prone to increase the selectivity of deep oxidation products

Table 3 Catalytic properties of the catalysts for isobutene oxidation at 420 °C[a]

Catalysts	Conversion (%)	Selectivity (%)						
		MAL	MAA	CO	CO_2	$C_3^=$	ACT	HAC
MoO_3	28.9	37.8	1.3	18.9	28.2	1.1	3.2	9.4
$MoV_{0.2}$-600-A	41.1	43.6	2.1	12.6	24.4	1.0	3.8	12.3
$MoV_{0.25}$-600-A	41.8	45.1	2.2	12.6	22.2	1.0	3.9	12.8
$MoV_{0.3}$-500-N	50.3	49.0	2.6	10.0	21.9	0.9	5.1	10.3
$MoV_{0.3}$-600-N	51.8	26.8	1.9	14.4	31.6	0.9	4.6	19.6
$MoV_{0.3}$-500-A	51.1	28.7	3.2	15.9	33.5	0.9	2.7	15.0
$MoV_{0.3}$-600-A	42.0	47.8	2.5	12.1	20.4	0.8	4.3	11.9
$MoV_{0.35}$-600-A	38.4	46.5	2.5	13.7	23.3	0.9	2.7	10.2

[a] Operating condition: GHSV = 1,800 mL h^{-1} g_{cat}^{-1}, $P = 101$ kPa

(CO_x). Under our test conditions, the sample of $MoV_{0.3}$-500-N achieved the best MAL selectivity (40.4%) at an isobutane conversion of 6.4%. Therefore, these Mo–V–O materials are hopefully further ameliorated to improve their catalytic performance for the selective oxidation of isobutane.

Acknowledgments This work was supported by the National Basic Research Program of China (2004CB217804) and the National Natural Science Foundation of China (20673046).

References

1. Mizuno N, Tateishi M, Iwamoto M (1996) J Catal 163:87
2. Mizuno N, Yahiro H (1998) J Phys Chem B 102:437
3. Langpape M, Millet JMM, Ozkan US, Boudeulle M (1999) J Catal 181:80
4. Cavani F, Mezzogori R, Pigamo A, Trifirò F (2003) Top Catal 23:119
5. Brückner A, Scholz G, Heidemann D, Schneider M, Herein D, Bentrup U, Kant M (2007) J Catal 245:369
6. Inoue T, Asakura K, Iwasawa Y (1997) J Catal 171:457
7. Paul JS, Urschey J, Jacobs PA, Maier WF, Verpoort F (2003) J Catal 220:136
8. Guan J, Jia M, Jing S, Wang Z, Xing L, Xu H, Kan Q (2006) Catal Lett 108:125
9. Guan J, Wu S, Jia M, Huang J, Jing S, Xu H, Wang Z, Zhu W, Xing H, Wang H, Kan Q (2007) Catal Commun 8:1219
10. Guan J, Wu S, Wang H, Jing S, Wang G, Zhen K, Kan Q (2007) J Catal 251:354
11. Schwaar RH (1993) Methacrylic acid and esters, Process Economics Program Report No. 11D, SRI International, 1993
12. Misono M, Nojiri N (1990) Appl Catal 64:1
13. Kung HH (1994) Adv Catal 40:1
14. Irigoyen B, Juan A, Castellani N (2000) J Catal 190:14
15. Li X, Iglesia E (2008) Appl Catal A: Gen 334:339
16. Solsona B, Vázquez MI, Ivars F, Dejoz A, Concepción P, López Nieto JM (2007) J Catal 252:271
17. Baca M, Aouine M, Dubois JL, Millet JMM (2005) J Catal 233:234
18. Imai H, Kamiya Y, Okuhara T (2007) J Catal 251:195
19. Sobalik Z, Gonzalez Carrazan S, Ruiz P, Delmon B (1999) J Catal 185:272
20. Borshch SA, Duclusaud H, Millet JM (2000) Appl Catal A: Gen 200:103
21. Tsuji H, Oshima K, Koyasu Y (2003) Chem Mater 15:2112
22. Millet JMM, Roussel H, Pigamo A, Dubois JL, Jumas JC (2002) Appl Catal A: Gen 232:77
23. Tu X, Sumida Y, Takahashi M, Niizuma H (2008) US Patent 7375052
24. Benderly A, Gaffney AM, Silvano MA (2008) US Patent 7361622
25. Dubois JL, Desdevises F, Serreau S, Vitry D, Ueda W (2008) US Patent 7345198
26. Dubois JL, Desdevises F, Serreau S, Vitry D, Ueda W (2008) US Patent 7332625
27. Machhammer O, Adami C, Hechler C, Zehner P (2008) US Patent 7321058
28. Ferguson EJ, Lucy AR, Roberts MS, Taylor DR, Williams BL (2007) US Patent 7262322
29. Gaffney AM, Song R (2006) US Patent 7074956
30. Gaffney AM, Song R (2006) US Patent 7053022
31. Gaffney AM, Song R (2004) US Patent 6746983
32. Bogan LE Jr, Han S, Jacobs BA, Kaiser FW, Klugherz PD, Lin M, Link RD III, Linsen MW (2004) US Patent 6710207
33. Chaturvedi S, Gaffney AM, Song R, Vickery EM (2003) US Patent 6656873
34. Watanabe H, Koyasu Y (2000) Appl Catal A: Gen 194–195:479
35. DeSanto P Jr, Buttrey DJ, Grasselli RK, Lugmair CG, Volpe AF, Toby BH, Vogt T (2004) Z Kristallogr 219:152
36. Ueda W, Vitry D, Katou T (2005) Catal Today 99:43
37. Guliants VV, Bhandari R, Swaminathan B, Vasudevan VK, Brongersma HH, Knoester A, Gaffney AM (2005) J Phys Chem B 109:24046
38. Kihlborg L (1969) Acta Chem Scand 23:1834
39. Ekstrom T, Nygren M (1972) Acta Chem Scand 26:1827
40. Botella P, López Nieto JM, Solsona B, Mifsud A, Márquez F (2002) J Catal 209:445
41. Bosch H, Sinot PJ (1989) J Chem Soc, Faraday Trans 1(85):1425
42. Parmaliana A, Arena F, Frusteri F (1997) Stud Surf Sci Catal 110:347
43. Adamski A, Sojka Z, Dyrek K (1999) Langmuir 15:5733
44. Paul JS, Jacobs PA, Weiss P-AW, Maier WF (2004) Appl Catal A: Gen 265:185
45. Védrine JC, Novakova EK, Derouane EG (2003) Catal Today 81:247
46. Novakova EK, Derouane EG, Védrine JC (2002) Catal Lett 83:177
47. Zhu Y, Lu W, Li H, Wan H (2007) J Catal 246:382